Development 138, 553-563 (2011) doi:10.1242/dev.055376

Sugar-free frosting, a homolog of SAD kinase, drives neural-specific glycan expression in the *Drosophila* embryo

Sarah Baas[1,2], Mary Sharrow[1], Varshika Kotu[1,2], Meg Middleton[1], Khoi Nguyen[1], Heather Flanagan-Steet[1], Kazuhiro Aoki[1] and Michael Tiemeyer[1,2,*]

SUMMARY

Precise glycan structures on specific glycoproteins impart functionalities essential for neural development. However, mechanisms controlling embryonic neural-specific glycosylation are unknown. A genetic screen for relevant mutations in *Drosophila* generated the *sugar-free frosting* (*sff*) mutant that reveals a new function for protein kinases in regulating substrate flux through specific Golgi processing pathways. Sff is the *Drosophila* homolog of SAD kinase, which regulates synaptic vesicle tethering and neuronal polarity in nematodes and vertebrates. Our *Drosophila sff* mutant phenotype has features in common with SAD kinase mutant phenotypes in these other organisms, but we detect altered neural glycosylation well before the initiation of embryonic synaptogenesis. Characterization of Golgi compartmentation markers indicates altered colocalization that is consistent with the detected shift in glycan complexity in *sff* mutant embryos. Therefore, in analogy to synaptic vesicle tethering, we propose that Sff regulates vesicle tethering at Golgi membranes in the developing *Drosophila* embryo. Furthermore, neuronal *sff* expression is dependent on transcellular signaling through a non-neural toll-like receptor, linking neural-specific glycan expression to a kinase activity that is induced in response to environmental cues.

KEY WORDS: Glycosylation, Golgi, Nervous system, *Drosophila*

INTRODUCTION

Essential aspects of neural development and function rely on the regulated expression of specific glycan structures. The involvement of glycans in neural cell function begins with neurectoderm differentiation, in which the elaboration of specific glycan structures on the Notch glycoprotein facilitates the differential ligand activation that drives cell fate selection (Okajima and Irvine, 2002). Subsequently, glycans expressed in developing and mature neural tissues impinge on other important cell signaling, migration, adhesion and synaptic functions (Matani et al., 2007). Several underlying molecular mechanisms for glycan function are well characterized, including the influence of N-linked polysialic acid on neural cell adhesion molecule (NCAM) interactions, the engagement of axonal glycosphingolipid glycans by a carbohydrate-binding protein on oligodendrocytes, and the activity-dependent deposition of glycosaminoglycans into perineuronal nets (Acheson et al., 1991; Matthews et al., 2002; Vyas et al., 2002). These instances, and others, reveal the prevalence of temporally and/or spatially regulated glycan expression. This is further supported by the existence of many anti-glycan antibodies (HNK-1, CAT, Jones, A2B5, FORSE-1, anti-HRP) that delineate subpopulations of neuronal or glial cells at various stages of development (Allendoerfer et al., 1999; Constantine-Paton et al., 1986; Jan and Jan, 1982; Kruse et al., 1984; Matthews et al., 2002; Sanes et al., 1986; Schnitzer and Schachner, 1982; Snow et al., 1987). Furthermore, aberrant glycan expression in humans is associated with various mild to severe pathologies (Dennis et al., 2009; Freeze, 2002; Lee et al., 2007; Michele and Campbell, 2003; Zak et al., 2002). Despite the overwhelming evidence for regulated glycan expression and for the significant consequences of disregulated glycan expression, the mechanisms that govern tissue-specific glycosylation are unknown, particularly during embryonic development.

We have previously reported that a mutation in an ectodermally expressed Toll-like receptor, *Tollo*, alters N-linked glycosylation in the developing *Drosophila* embryonic nervous system (Seppo et al., 2003). This defect was detected as loss of staining with antibodies that recognize a family of structurally related N-glycans, known as HRP epitopes, which are normally expressed in a restricted set of embryonic tissues (Jan and Jan, 1982; Snow et al., 1987). The *Tollo* mutation specifically abolishes HRP-epitope expression in neural tissue although Tollo is not expressed in neural cells that carry HRP epitopes. Rather, it is expressed and functions within non-neural ectodermal cells that surround differentiating neurons, establishing the basis for a transcellular paracrine signaling pathway that drives neuron-specific glycosylation (Seppo et al., 2003). Such transcellular signaling might drive cell-specific glycan expression through altered transcription of glycan biosynthetic genes (glycosyltransferases, glycan processing enzymes, etc.) or through mechanisms that modify trafficking through specific glycoprotein processing pathways. The relative contribution of altered transcription and altered cellular organization to tissue-specific glycan expression is completely unresolved in any biological context. To address this lack of knowledge and to identify the unknown components of the Tollo transcellular signaling mechanism, we undertook a random mutagenesis screen for genes that specifically affect HRP-epitope expression in the *Drosophila* embryo. Here, we describe an informative mutation recovered from this screen called *sugar-free frosting* (*sff*), the phenotype of which reveals the importance of regulated Golgi dynamics for neuron-specific glycan expression. Our

[1]Complex Carbohydrate Research Center, University of Georgia, 315 Riverbend Road, Athens, GA, 30602-4712, USA. [2]Department of Biochemistry and Molecular Biology, University of Georgia, B122 Life Sciences Building, Green Street, Athens, GA, 30602-4712, USA.

*Author for correspondence (mtiemeyer@ccrc.uga.edu)

Accepted 22 November 2010

sff mutation, which is the first described disruption of a *Drosophila* homolog of SAD kinase, interacts genetically with *Tollo* and modulates glycan complexity in neurons that are receptive to the *Tollo* transcellular signaling pathway (Crump et al., 2001; Inoue et al., 2006; Kishi et al., 2005). Our results lead us to propose a new paradigm in which tissue-specific glycan expression is sculpted by the relative activities of multiple protein kinases, each acting to facilitate flux through specific Golgi processing pathways.

MATERIALS AND METHODS

Reagents

Probes for immunohistochemistry and immunofluorescence used were: rabbit anti-HRP (1:2000 for embryos, 1:1000 for larvae), HRP-Concanavalin A (ConA; 1:100), HRP-conjugated goat anti-rabbit (1:1000) and goat anti-mouse (1:1000) antibodies from Jackson Laboratories; monoclonal antibodies 1D4 (anti-Fas2; 1:3), nC82 (anti-Brp; 1:100) and 22C10 (1:5) from the Developmental Studies Hybridoma Bank (DHSB, University of Iowa, IA, USA); biotin-conjugated PNA (peanut lectin; 5 μg/ml) obtained from Vector Laboratories; anti-GM130 (1:1000) monoclonal antibody obtained from Abcam; Alexa-conjugated secondary antibodies (Alexa 488, 568 and 633; 1:500), rabbit anti-GFP (cross-reactive with YFP; 1:5000) and PROLONG anti-fade obtained from Molecular Probes; TRITC-Phalloidin (1:100) obtained from Invitrogen. PNGaseA was from Calbiochem; trypsin and chymotrypsin were from Sigma.

Drosophila mutagenesis and transgenesis

Males of genotype w^{1118}; +; + were treated with 25 mM ethyl methanesulfonate and mated en masse to females of the genotype w^{1118}; *Kr*/CyO; *D*/TM6b. Individual male progeny heterozygous for the second and third chromosome markers were backcrossed to w^{1118}; *Kr*/CyO; *D*/TM6b females to create lines that carried mutagenized second or third chromosomes. Progeny from each individual line were sib-mated to give embryo collections that were stained with anti-HRP antibody. Lines showing altered HRP-epitope expression were subsequently stained with Concanavalin A. Lines that were deficient in anti-HRP staining but normal for Concanavalin A staining were maintained.

All mapping, balancer, deletion and marked chromosome stocks were obtained from the Bloomington *Drosophila* Stock Center at Indiana University. Two *Tollo* mutant lines were used. One is as previously described (Seppo et al., 2003), and the other ($tollo^{c5}$) was obtained from B. Charroux and J. Royet (IBDML, Marseille, France). For confocal characterization of the medial/trans Golgi, the YFP reporter carried by the Golgi-YFP line obtained from Bloomington was recombined onto the sff^{B22} chromosome (third chromosome mutation). Therefore, for Golgi characterization, wild type refers to the parental w^{1118}; +; Golgi-YFP line. Otherwise, wild type refers to *OreR*.

Drosophila lines expressing Sff (*CG6114*) under Gal4/UAS control were generated by P-element-mediated insertional transgenesis. Vector containing *CG6114* cDNA missing 209 bp of coding sequence (including the start codon) was obtained from Berkeley *Drosophila* Genome Project (clone GH13047 in pOT2). The insert was excised with *Eco*RI/*Xba*I and the missing coding sequence plus 97 bp of the 5′UTR was recovered by PCR from wild-type cDNA. Taking advantage of an endogenous *Eco*RI site, both sequences were ligated and cloned into the pBl(KS+) vector (Stratagene) and the integrity of the PCR-amplified region was verified by sequencing. The resulting full-length insert was subcloned into pUAST. Transformant lines were generated by co-injection of pUAST-*CG6114* and wcΔ2-3 into w^{1118} embryos by standard procedures (Brand et al., 1994). A second chromosome insertion was homozygosed into sff^{B22} and crossed to ELAV-Gal4; sff^{B22} homozygotes. Progeny embryos were stained with anti-HRP antibody to assess rescue of the *sff* phenotype.

Immunohistochemistry, immunofluorescence and confocal colocalization

Embryos from overnight collections were dechorionated, fixed, devitellinized and stained with antibodies using blocking conditions and wash buffers as previously described (Patel, 1994; Seppo et al., 2003). For histochemical probes (antibodies and ConA), Nomarski (differential interference contrast) and light micrographs were obtained on a Zeiss Axioskop microscope fitted with a Retiga 2000R CCD camera (Q Imaging, Surrey, Canada). Neuromuscular junction (NMJ) morphology was assessed in wandering third instar larvae raised at 18°C. Larval dissections were performed as previously described (Kaufmann et al., 2002). The NMJ at muscles 6 and 7 (abdominal segments 3 and 4) were imaged by laser scanning confocal microscopy (LSC, Olympus FV1000) with a 40× (N.A. 1.30) oil objective. Stacks of optical sections were collected in the *z*-dimension; step size, based on the calculated optimum, was 0.50 μm. Maximum intensity projections were assembled using NIH Image J. Golgi imaging was performed on an Olympus FV1000 LSC microscope with a 60× (N.A. 1.42) oil objective. Images were acquired in the *z*-dimension with step size of 0.45 μm. Laser intensity, slice thickness and all other acquisition parameters were identical for imaging wild-type and mutant embryos. Image analysis was accomplished offline with the Slidebook software package (Intelligent Imaging Innovations, Denver, CO, USA) on non-compressed *z*-stacks. Confocal stacks were adjusted for background and channel overlap using the software supplier's recommended algorithms. Total and colocalized fluorescence intensity for each marker was quantified within selected regions of interest.

In situ hybridization

To prepare the anti-sense probe for *CG6114* (*sff*), wild-type genomic sequence corresponding to 2581 bp of the *CG6114* 3′ UTR was amplified by PCR and cloned into PCR 2.1 TOPO vector (Invitrogen). Clones were recovered bearing the insert in both sense and anti-sense orientations relative to the T7 promoter (Kopczynski et al., 1996). Digoxigenin-11-UTP-labeled RNA was prepared by in vitro transcription using T7 polymerase and DIG RNA Labeling Kit (Roche). In situ hybridization of anti-sense probes (see Table S2 in the supplementary material) to wild-type embryos from overnight collections (25°C) was detected by alkaline phosphatase with BCIP/NBT (5-bromo-4-chloro-3′-indolylphosphate/nitro-blue tetrazolium).

Glycan analysis

Total N-glycans were prepared from overnight embryo collections (25°C) by PNGaseA digestion of tryptic/chymotryptic peptides as previously described (Aoki et al., 2007). Following permethylation, total glycan profiles were acquired by mass spectrometry (MS) using nanospray ionization interfaced to a linear ion trap instrument (NSI-MS^n on an LTQ Ion Trap, Thermo-Fisher). The Total Ion Mapping (TIM) functionality of the instrument control and data acquisition software (Xcalibur, v2.0) was used to acquire full MS and MS/MS spectra (~700 spectra per sample), which were manually interpreted to assign glycan structures and to quantify relative glycan prevalence. Ambiguities were resolved by acquisition of spectra at MS^3-MS^4 as needed.

Proteomic analysis by liquid chromatography with tandem mass spectrometry (LC-MS/MS)

Proteins from adult head lysates were reduced, alkylated, digested with sequencing grade trypsin (Promega) and subjected to proteomic analysis by LC-MS/MS (Lim et al., 2008). Two-dimensional RP/RP-HPLC (reverse phase/reverse phase high pressure liquid chromatography) was performed to separate the total peptide mixture into five fractions (F1-5) based on hydrophobicity. Fractionated peptides were loaded off-line onto a nanospray tapered capillary column emitter and LC-MS/MS analysis was performed on an LTQ Orbitrap mass spectrometer (Discovery, Thermo-Fisher) with a Surveyor MS pump plus (Thermo Scientific). As the five RP-fractions each contain peptide pools that possess different average hydrophobicities (increasing from F1-5), separate gradient elution conditions were employed for LC-MS/MS analysis of each fraction (see Fig. S6 in the supplementary material) in order to maximize peptide resolution. MS/MS spectra (36% normalized collision energy) were triggered upon detection of any mass-to-charge ratio (m/z) signal that corresponded to any entry into a parent mass list of theoretical CG6114 tryptic peptides, allowing for up to 2 missed cleavages, oxidized methionine, alkylated cysteine and charge states to +3. MS/MS data was searched against the Fly database (*Drosophila melanogaster*, 8-31-09) from Swiss Prot to which CG6114 was added, and against the reverse of this

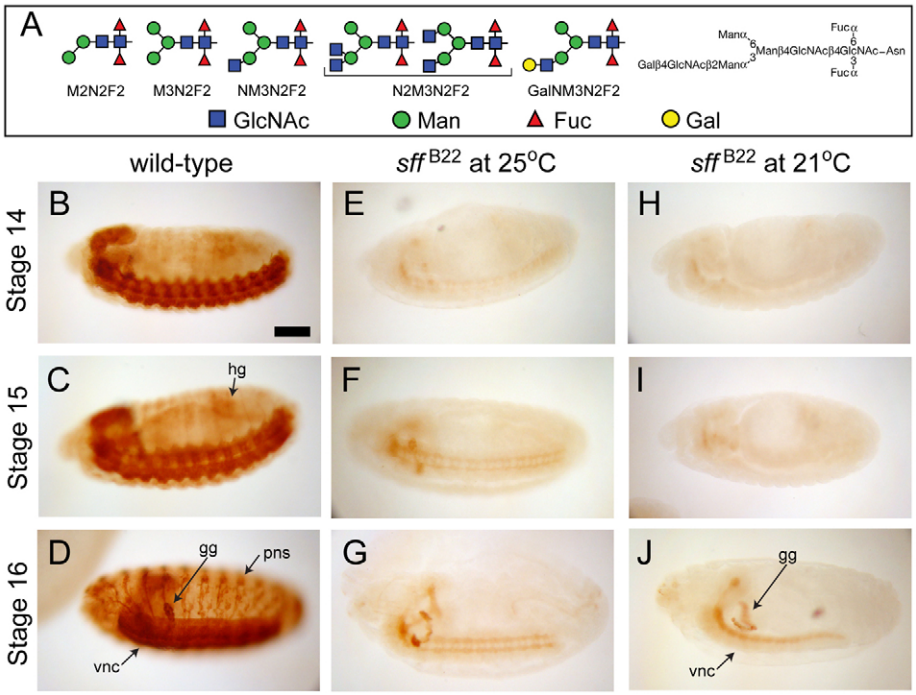

Fig. 1. HRP-epitope expression is decreased in *sff*^{B22} embryos. (**A**) HRP epitopes of the *Drosophila* embryo are N-linked glycans that share an antigenic determinant: Fuc in α3-linkage to the innermost GlcNAc of the chitobiose core. Graphical representations of monosaccharides and glycan structures in all figures are in accordance with the recommendations of the Consortium for Functional Glycomics. (**B-D**) Anti-HRP staining of wild-type *Drosophila* embryos is shown at progressively later stages, anterior to the left. HRP epitope is visible along the ventral nerve cord (vnc), the hindgut (hg) and the garland gland (gg). Peripheral nervous system (pns) staining is first apparent at Stage 14, but clearly detectable at stage 16. (**E-G**) In *sff*^{B22} embryos at 25°C, staining is only detected at the dorsal surface of the nerve cord, along the axon scaffold and in the garland gland. Hindgut staining is not detected. (**H-J**) At 21°C, the appearance of residual HRP epitope in the *sff* mutant is delayed in comparison with that observed in mutants at 25°C. Scale bar: 60 μm for B-J.

database to assess false discovery. SEQUEST parameters were set with a mass tolerance of 30 ppm, fragment ion cutoff of 0.1% and allowance for 2 missed cleavages.

Geotaxis behavior

Males that had been raised for 8 days at 25°C or 18°C were placed individually into empty plastic culture vials containing no media. Following dark adaptation for one hour (under red safelights) at 18°C, the test subjects were gently tapped to the bottom of the vial. The elapsed time for the subject to climb to a mark 3 cm up the side of the vial was recorded. For subjects that did not reach the pre-determined height, the trial was terminated after 2 minutes and the elapsed time was scored as 120 seconds.

Transcript analysis by qRT-PCR

Overnight embryo collections were dechorionated and total RNA was isolated using RNAeasy (Qiagen). cDNA was prepared from 5 μg of total RNA using the Superscript III First-Strand synthesis system (Invitrogen). Quantitative RT-PCR was performed as previously described, using SYBR green for detection (Nairn et al., 2007).

RESULTS

Decreased expression of HRP epitopes in *sugar-free frosting* mutant embryos

Antibodies generated against the plant glycoprotein horseradish peroxidase (HRP) cross-react with specific asparagine-linked oligosaccharide structures expressed in the nervous system of many arthropods (Jan and Jan, 1982; Snow et al., 1987). These N-glycans, collectively known as HRP epitopes, carry α3- and α6-linked fucose (Fuc) on the innermost N-acetylglucosamine (GlcNAc) of the chitobiose core (GlcNAcβ4GlcNAc, Fig. 1A). Although the recognized structures are difucosylated, α3-linked Fuc is the dominant antigenic determinant (Kurosaka et al., 1991). HRP epitopes are expressed throughout the entire *Drosophila* life cycle (Aoki et al., 2007; Fabini et al., 2001). In the embryo, anti-HRP staining was evident in the ventral nerve cord and peripheral nervous system, as well as in a limited set of non-neural tissues, including the garland gland and the hindgut (Fig. 1B-D).

The restricted distribution of HRP epitopes provides a platform for identifying genes that govern tissue-specific glycan expression. Therefore, we undertook a random chemical mutagenesis screen to harvest mutations that specifically alter expression of HRP epitopes without generally affecting N-linked glycosylation. Embryos from the F2 generation derived from mutagenized male founders were stained with anti-HRP antibody and examined for loss of HRP epitopes. Mutant lines that exhibited altered HRP-epitope expression were stained with Concanavalin A (ConA), which reports the presence of high-mannose oligosaccharides, to assess the integrity of the core glycosylation machinery.

One mutation recovered from the screen, initially designated B22, was a semi-viable third chromosome line with substantial loss of all neural HRP-epitope expression but with normal ConA staining (Fig. 1 and see Fig. S1 and Table S1 in the supplementary material). Residual staining was apparent in late stages within the axon scaffold of the ventral nerve cord. This neural staining was restricted to the dorsal aspect of the nerve cord and gave the appearance of a frosting-like layer of epitope, prompting us to name the mutation '*sugar-free frosting*' (*sff*). At reduced temperature (21°C), the onset of residual epitope expression was delayed until slightly later stages than that observed at 25°C (Fig. 1H-J). In non-neural tissues, hindgut staining was severely reduced although the garland gland retained HRP-epitope expression in *sff*^{B22} embryos.

The *sugar-free frosting* mutation maps to the *Drosophila* homolog of *SAD kinase*

Recombination mapping placed *sff* distal to *scarlet* (*st*) on the left arm of the third chromosome. Deletion mapping in the interval between *st* and the left end of the chromosome identified a single deletion (Δ*brm*^{11}) that failed to complement the *sff* mutation. Embryos of the genotype *sff*^{B22}/Δ*brm*^{11} displayed a more severe HRP phenotype than did *sff* homozygotes, and Δ*brm*^{11} deletion homozygous embryos lacked all HRP epitopes, indicating that the *sff*^{B22} allele is hypomorphic with regard to the induction of HRP-

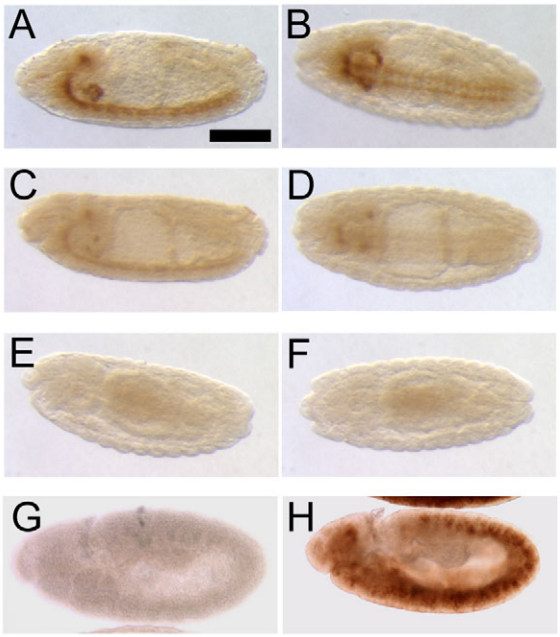

Fig. 2. The *sff* mutation is uncovered by the Δ*brm*^{11} deficiency and *sff*^{B22} is an hypomorphic allele that is rescued by transgenic expression of CG6114. (**A-F**) A late stage 14 *sff*^{B22} embryo (anterior to the left) stained with anti-HRP antibody exhibits epitope distribution characteristic for the mutant (A,B). A late stage 14 embryo of the genotype *sff*^{B22}/Δ*brm*^{11} (C,D) shows reduced staining compared with the *sff*^{B22} homozygote (A,B). A late stage embryo homozygous for the Δ*brm*^{11} deletion shows complete loss of HRP epitope (E,F). Embryos in A-D were processed in parallel. A, C and E show lateral views; B, D and F show ventral views. (**G**,**H**) Lateral views of stage 12 embryos of genotype elav-Gal4; +/+; *sff*^{B22}/*sff*^{B22} (G) and elav-Gal4; UAS-*CG6114*/+; *sff*^{B22}/*sff*^{B22} (H), demonstrating rescue of HRP-epitope expression by transgenic Sff. Scale bar: 120 μm for all panels.

epitope expression (Fig. 2A-F). Loss of hindgut and garland gland HRP epitopes in the deletion homozygote implies a role for *sff* in the subset of non-neural tissues that normally express these glycans. We characterized the deletion breakpoints of the non-complementing Δ*brm*^{11} deletion and of an overlapping, but complementary, deletion Δ*th*^{102} (Mathew et al., 2009). Comparison of these breakpoints identified *CG6114* as the only gene deleted by Δ*brm*^{11} but not by Δ*th*^{102} (see Fig. S2A in the supplementary material). Genomic sequencing of the *CG6114* locus in the *sff*^{B22} mutation identified a single nucleotide change (G to A) in a consensus AP-1 binding site 261 bp upstream of the predicted transcript start (see Fig. S2B in the supplementary material). The detected nucleotide change prevented the sequence from being recognized as an AP-1 binding site above threshold (85% confidence) by the TFSearch algorithm (v1.3) utilizing the TRANSFAC database (Heinemeyer et al., 1998). The *CG6114* sequence is highly homologous to a serine-threonine protein kinase previously identified as Synapses of Amphids Defective (SAD-1 Kinase) in *Caenorhabditis elegans* and mammals (SAD-1/2) (see Fig. S3 in the supplementary material). All canonical amino acid residues essential for serine-threonine kinase catalytic activity are conserved in the CG6114 coding sequence (Hanks and Hunter, 1995). To verify that the reduction in HRP-epitope expression is due to decreased CG6114 function, we generated a transgenic line expressing *CG6114* cDNA (UAS-*CG6114*) driven by the pan-neural driver, *elav*-Gal4. The UAS-*CG6114* transgene was sufficient to rescue neuronal HRP-epitope expression in *sff*^{B22} embryos (Fig. 2G,H).

Sff is expressed in embryonic neurons and is decreased in the *sugar-free frosting* mutant

By in situ hybridization, mRNA for *sff* was detected in the embryonic ventral nerve cord and peripheral sensory clusters in the ventral and lateral ectoderm (Fig. 3A-E) (Kopczynski et al., 1996). If present in the hindgut or garland gland, *sff* mRNA was below the current detection threshold for our in situ analysis. Therefore, despite complete loss of HRP epitopes in Δ*brm*^{11} homozygotes (see Fig. 2E,F), additional tissue-specific regulatory mechanisms are likely to contribute to HRP-epitope expression in non-neural tissues. Consistent with our genetic characterization of the *sff*^{B22} allele as a hypomorph, mRNA for *sff* was reduced, but not eliminated, in the mutant nervous system (Fig. 3B,E, quantified in Fig. 4). The cells expressing *sff* mRNA were neuronal as hybridization signal was detected within cells that were also positive for the neuron-specific mAb 22C10 (see Fig. S4 in the supplementary material). Expression of *sff* mRNA was first visible along the midline of the embryo at stage 11, prior to the initiation of synapse formation in the embryo and roughly coincident with the initial appearance of HRP epitopes and transcripts for FucTA, the α3-fucosyltransferase that synthesizes HRP epitopes (see Fig. S5 in the supplementary material) (Rendic et al., 2006; Rendic et al., 2010). As neurons continued to differentiate and extend axons, *sff* mRNA levels increased across the maturing nerve cord. In peripheral sensory clusters, mRNA was detected as early as stage 13, prior to significant accumulation of HRP epitopes and before synaptic contact had been made between sensory afferents and their targets in the ventral nerve cord, which generally begins during stage 16 (Martin et al., 2008; Merritt and Whitington, 1995). Consistent with reduced *sff* mRNA expression in *sff*^{B22}, proteomic analysis by LC-MS/MS demonstrated reduced Sff protein levels in *sff*^{B22} adult heads, which also exhibited reduced HRP-epitope expression (see Table S3 and Fig. S6 in the supplementary material) (Lim et al., 2008).

Sff Interacts with Tollo

HRP epitope loss in *sff*^{B22} suggested that Sff might act in the transcellular signaling pathway defined by Tollo (Seppo et al., 2003). As heterozygous embryos, *sff*^{B22} or *Tollo* mutations (over a wild-type chromosome) exhibited normal HRP-epitope expression. As homozygous embryos, the *sff* phenotype was not identical to the *Tollo* phenotype. Hindgut staining was absent and garland gland staining was reduced in *sff*^{B22} but not in the *Tollo* mutant, whereas nerve cord staining was completely absent in *Tollo* mutants but still faintly present in *sff*^{B22}. Transheterozygous embryos of the genotype *sff*^{B22}, *Tollo*$^{+}$/*sff* $^{+}$, *Tollo*$^{-}$ possessed aspects of both phenotypes; faint residual nerve cord staining was seen along with rescue of hindgut HRP epitopes (Fig. 4A-D). This composite phenotype is consistent with an interaction in which reduction of either gene dose results in sensitization for both phenotypes. Thus, *sff*^{B22} enhanced partial loss of *Tollo*, and vice versa, indicating functional interactions between the two genes. Significantly, *Tollo* mutant embryos exhibited reduced *sff* transcripts, both in our previously described *Tollo* mutant (Fig. 4E,F) and in another mutant allele (*tollo*^{c5}) generated by FLP-FRT recombination (B. Charroux and J. Royet, personal communication), which also exhibits reduced HRP-epitope expression (Fig. 4G and see Fig. S7 in the supplementary material)

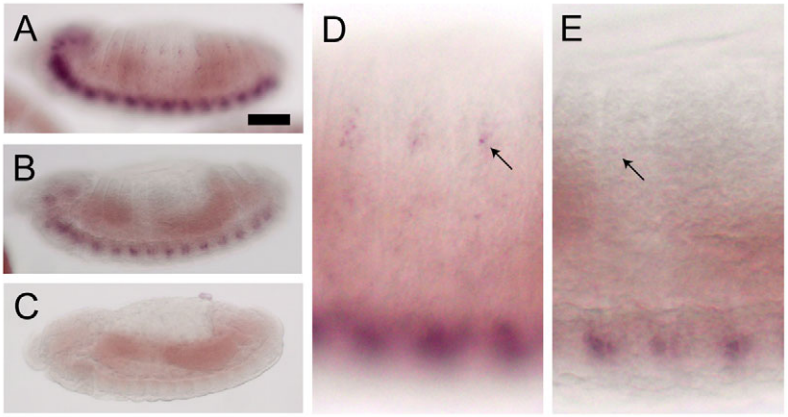

Fig. 3. *Drosophila sff* mRNA is expressed in the embryonic nervous system and is reduced in *sff*^{B22}. (**A-E**) In situ hybridization (ISH) with anti-sense probe for *CG6114* (*sff*) to late stage 13 wild-type embryo (A,D) reveals prominent message expression in the ventral nerve cord and in sensory neurons in the PNS (arrows in D). ISH on a late stage 13 *sff*^{B22} embryo shows decreased mRNA levels in the ventral nerve cord (B) and PNS (E). Arrow indicates low staining in sensory neurons of the PNS. No hybridization was observed with the sense probe (C; late stage 13 wild-type embryo). Anterior is to the left. Embryos presented in all panels were processed in parallel. Scale bar: 60 μm for A-C; 15 μm for D,E.

(Parks et al., 2004). Therefore, ectodermal Tollo signaling influences neural glycosylation, at least in part, by driving expression of Sff in differentiating neurons.

Behavioral and neuromuscular deficits in the *sugar-free frosting* mutant

Homozygous *sff*^{B22} adults were reluctant to climb up the side of their culture vials, a phenotype previously described for *Tollo* mutants (Seppo et al., 2003). In general, *sff*^{B22} adults righted themselves when knocked to the bottom of an empty culture vial and exhibited reasonable locomotion once movement was initiated, but failed to move in a directed fashion away from gravity (see Movie 1 in the supplementary material). We quantified this negative geotaxis defect by measuring the time required for individual adults to climb to a pre-designated height (Fig. 5A). Wild-type adults quickly reached the target height; 81% succeeded within 15 seconds at 25°C. However, *sff* mutants tarried and often never reached the designated height before the trial was ended at 2 minutes; only 36% succeeded within 15 seconds at 25°C. As with anti-HRP antibody staining, the geotaxis phenotype was more pronounced at reduced temperature.

Because motility requires a functional NMJ, we investigated the status of the NMJ in third instar larvae. In *sff* mutants, the NMJ was considerably less complex (Fig. 5B-E), with a significant reduction in both bouton and primary branch number. NMJ morphology is also disrupted in the *C. elegans SAD-1* mutant, with poor alignment of synaptic vesicles at the active zone complex. Despite deficient vesicle tethering, the presynaptic specializations that make up the active zone are well structured in the *C. elegans* mutant (Crump et al., 2001). To assess in a similar manner the integrity of the active zone scaffold in our *Drosophila sff* mutant, we examined the distribution of the Bruchpilot protein (Brp), which participates in the formation of T-bars (the electron-dense projections upon which synaptic vesicles are tethered) at the NMJ (Wagh et al., 2006). The distribution of Brp within individual boutons was unaltered in *sff* mutant NMJs compared with wild type (Fig. 5F,G). Therefore, reduced Sff in *Drosophila*, similar to reduced SAD-1 in *C. elegans*, did not affect the structural integrity of the presynaptic scaffold required for vesicle release.

Increased N-linked glycan complexity in *sugar-free frosting* mutant embryos

N-linked glycan biosynthesis and processing in *Drosophila* proceeds through steps that are well conserved across the animal kingdom (Fig. 6A). A major difference between *Drosophila* and vertebrate glycan processing is the activity of an N-acetylhexosaminidase, known as Fused Lobes (Fdl), which removes the GlcNAc residue added by N-acetylglucosaminyltransferase-I (GlcNAcT1). The Fdl enzyme

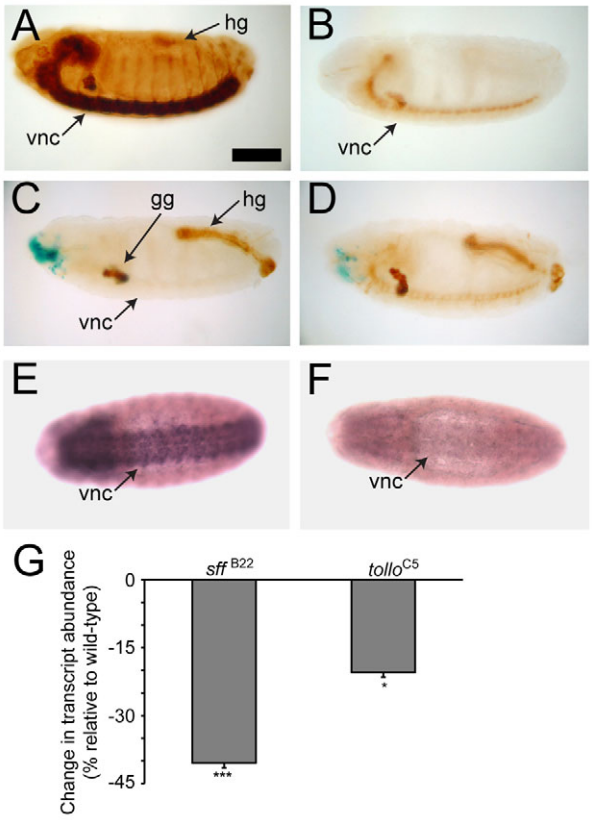

Fig. 4. *sff* interacts with *Tollo* and expression of *sff* mRNA is dependent on *Tollo*. (**A**) Wild-type embryos and embryos heterozygous for either *Tollo* or *sff*^{B22} are identical in appearance, with strong staining of the ventral nerve cord (vnc), garland gland (gg) and hindgut (hg). (**B**) Embryos homozygous for the *sff*^{B22} mutation exhibit reduced vnc and hg staining. (**C**) Embryos homozygous for loss of *Tollo* lack vnc staining but retain gg and hg expression of the HRP epitope. (**D**) Embryos that are transheterozygous for both *sff*^{B22} and *Tollo* have a composite staining phenotype, indicating functional interactions between the two genes. (**E**,**F**) In situ hybridization of antisense probe for *sff* in wild-type (E) and *Tollo* mutants (F) indicates that Tollo signaling induces neuronal expression of *sff* mRNA. Scale bar: 90 μm for A-F. (**G**) qRT-PCR of *sff* transcript levels in *sff* (*sff*^{B22}) and *Tollo* (*tollo*^{c5}) mutant embryos, relative to wild type *P<0.05, ***P<0.01; mean ± s.e.m. for three independent analyses.

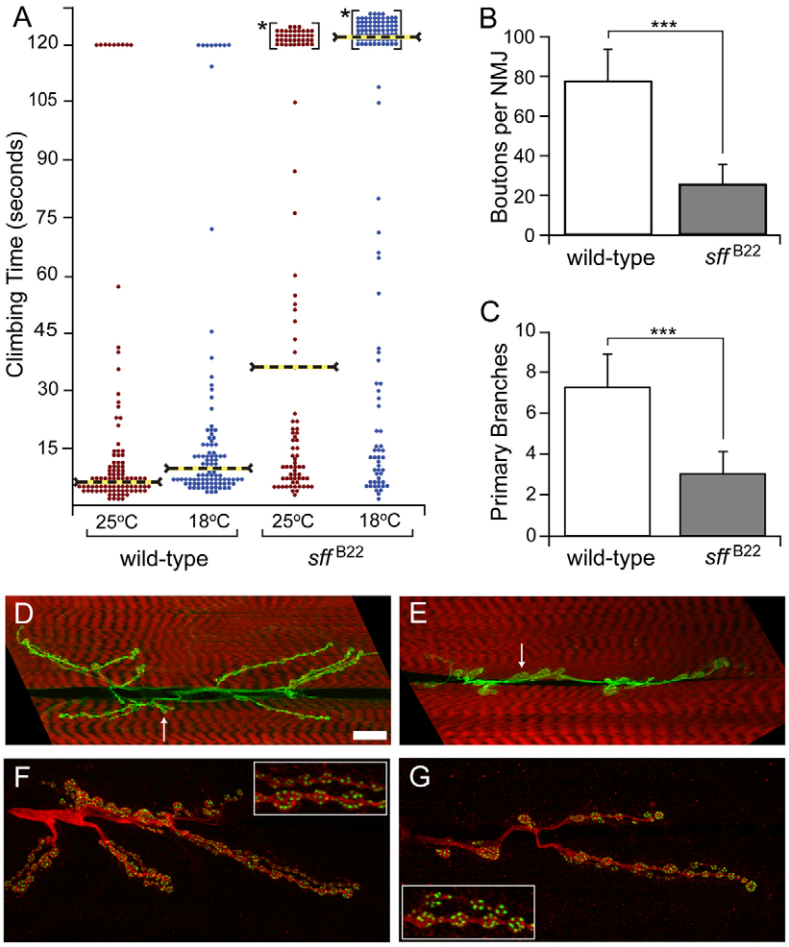

Fig. 5. *Sff* mutants exhibit behavioral and neuromuscular junction (NMJ) phenotypes. (**A**) *Drosophila Sff* mutants are deficient in negative geotaxis. Each dot represents the climbing time for a single adult male to reach a pre-specified height. Dashed lines indicate the median climbing time for the indicated population. Individuals that did not reach the threshold height within 120 seconds are binned together (*). For all populations, *n*=100-122 males. (**B**,**C**) The number of boutons and the number of primary nerve branches are significantly decreased at the NMJ in the sff^{B22} mutant. Data are mean ± s.e.m. ***P<0.001; *n*=25 wild-type, *n*=7 sff^{B22} for panel B and *n*=23 wild-type, *n*=22 sff^{B22} for panel C. (**D**,**E**) Compressed *z*-stacks from confocal images of the larval NMJ in wild type (D) and sff^{B22} (E) present the gross change in morphology resulting from decreased Sff function (red, phalloidin; green, anti-HRP). In addition to decreased bouton number and decreased nerve terminal branching, the sff^{B22} NMJ is characterized by enlarged boutons (arrows in D and E). (**F**,**G**) The distribution of active zone complexes is not altered by the *sff* mutation. Wild-type (F) and sff^{B22} (G) larval NMJs were stained with anti-Bruchpilot (green) and anti-HRP (red). Neither the size of Bruchpilot complexes nor the number of complexes per bouton was significantly altered (insets). In panels D-G anti-HRP staining delineates the full extent of the axonal arborization. Despite reduced HRP epitope in embryos and larvae, anti-HRP antibody staining is co-extensive with mAb 1D4 staining, another well-established NMJ marker (see Fig. S8 in the supplementary material). Scale bar: 20 μm for D,E; 15 μm for F,G; 4 μm for insets in F,G.

drives the predominance of paucimannose structures in the wild-type *Drosophila* glycan profile by converting NM3N2 glycans to M3N2, thereby eliminating the precursor pool for hybrid or complex structures (Leonard et al., 2006). Limited expression of branching and terminal glycosyltransferases, such as GlcNAcT2, GlcNAcT4, GalT, GalNAcT or SiaT, also restrict the capacity for generating complex structures (Haines and Irvine, 2005; Koles et al., 2004; Repnikova et al., 2010; Sarkar et al., 2006). HRP epitopes represent less than 1% of all N-linked glycans in the *Drosophila* embryo (Aoki et al., 2007). Therefore, anti-HRP antibody staining reports the status of a limited set of N-glycan processing pathways.

To comprehensively identify glycan expression changes induced by the *sff* mutation, total N-linked glycan profiles of *sff* and wild-type embryos were analyzed by mass spectrometry. High mannose and paucimannose glycans together accounted for almost 90% of the total profile in wild-type (89.5%) and *sff* mutant (85.5%) embryos, indicating that the dominant glycan processing pathways are largely unaffected by the *sff* mutation. (see Table S4, structures 1-13, in the supplementary material). However, the prevalence of the M5N2 structure, an essential precursor for paucimannose, hybrid and complex glycan production, was reduced in the *sff* mutant (Fig. 6B). The decrease in M5N2 was mirrored by an increase in M3N2, a paucimannose glycan production of which requires Fdl, indicating robust activity of the processing hexosaminidase in *sff* embryos. Hybrid and complex glycans together made up 9.6% of the total profile in wild-type and 11.1% in *sff* embryos (see Table S4, structures 14-25 and 31-42, in the supplementary material). This modest increase in the prevalence of processed glycans, equivalent to a shift of 1.5% of the total glycan profile in the *sff* mutant, was more dramatic for a subset of individual complex structures (Fig. 6C). For example, the N2M3N2 glycan, a biantennary non-fucosylated structure, was increased by 30% and the N3M3N2F glycan, a triantennary core-fucosylated structure, was increased by 385% in the *sff* mutant. As expected, glycans bearing α3-linked Fuc were significantly reduced in *sff* embryos (54% reduction overall), accounting for 0.5% less of the total glycan profile than in wild type (Fig. 6D). However, one HRP epitope, the complex biantennary N2M3N2F2 glycan, was more prevalent in *sff* than in wild-type embryos. This difucosylated structure, like the non-HRP complex structures that were also increased in *sff* mutants, requires the activity of GlcNAcT2 or GlcNAcT4 (Fig. 6A), indicating that the *sff* mutation increases the flux of glycan processing towards greater complexity. Our previous structural characterization of the glycans expressed in *Tollo* mutant embryos also demonstrated increased prevalence of complex non-fucosylated glycans in addition to reduced expression of HRP epitopes, consistent with both genes acting within an intersecting pathway (Aoki et al., 2007).

To determine if the shifted glycan profile in *sff* results from altered transcription of genes encoding glycosyltransferases or glycan processing enzymes, we performed qRT-PCR in order to quantify transcript levels for genes encoding Fdl, FucTA, GlcNAcT1, GlcNAcT2 and a GlcNAcT4 candidate (*CG9384*) relative to *GAPDH1* (Fig. 6E). *FucTA* transcription was modestly reduced in sff^{B22} (30%), although the reduction in message was

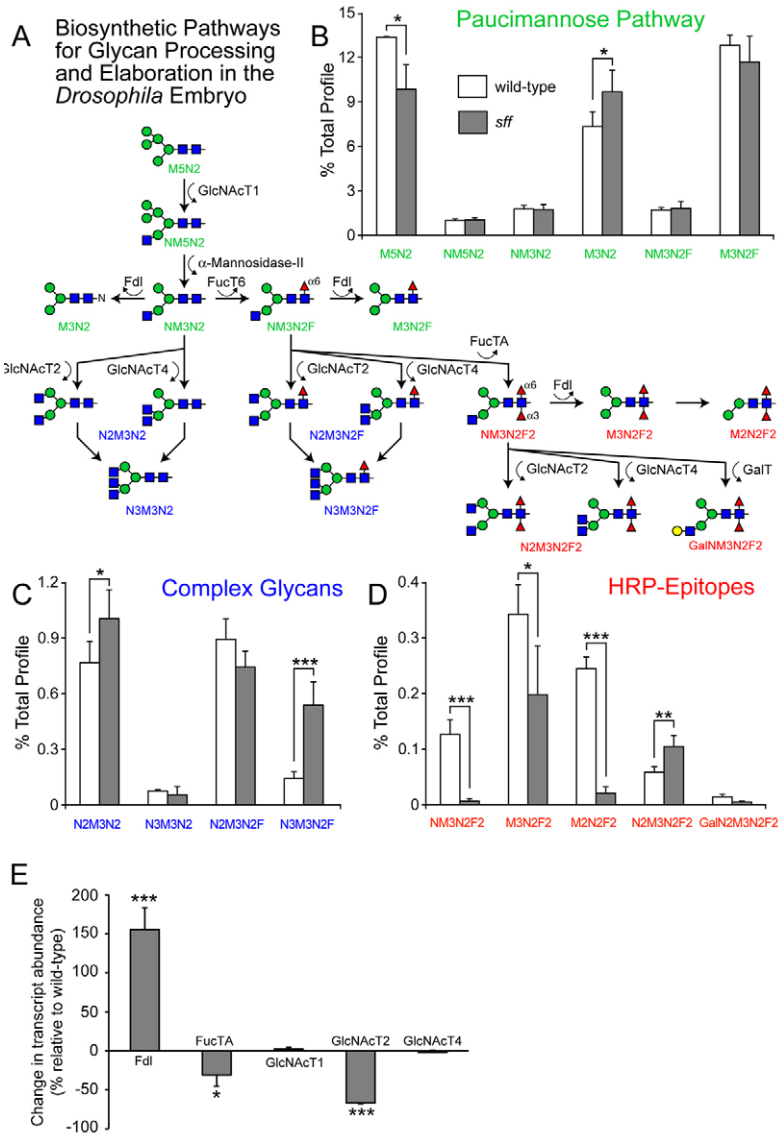

Fig. 6. The N-linked glycan profile of the *sff*^{B22} mutant is deficient in HRP epitopes and shifted towards greater complexity. (**A**) N-linked glycan processing in *Drosophila* proceeds through steps that are well conserved across animal species. See Fig. 1 for key to graphical representation of structures. GlcNAcTransferase-1 (GlcNAcT1) transfers a GlcNAc residue to the trimmed high-mannose structure M5N2. Subsequent removal of Man residues by Golgi mannosidases produces NM3N2, a structural node that feeds into three separate pathways. The Fused Lobes hexosaminidase (Fdl) can remove the GlcNAc added by GlcNAcT1 to generate the paucimannose glycan M3N2. Alternatively, NM3N2 can be branched by the action of another GlcNAcTransferase (GlcNAcT2 or GlcNAcT4) to produce complex glycans that are resistant to degradation by Fdl. The NM3N2 glycan is also a substrate for α6-fucosylation (FucT6) and subsequent branching by GlcNAcT2 or GlcNAcT4. Addition of α3-Fuc residues (FucTA) generates HRP epitopes. (**B-D**) The prevalences of the indicated glycans are given as the percent that they contribute to the total profile of N-linked glycans (% Total Profile, see Table S4 in the supplementary material for full glycan profiles). (**E**) qRT-PCR of glycogene transcript levels in *sff* mutant embryos relative to wild type **P*<0.05, ***P*<0.02, ****P*<0.01. Values are the mean ± s.e.m. for three independent analyses in panels B-E.

disproportionate to the larger reduction in HRP-epitope expression (54%). Furthermore, the increase in *Fdl* transcripts and the decrease in *GlcNAcT2* transcripts were inconsistent with the shift in the total glycan profile towards greater complexity and reduced HRP-epitope production. Similar transcript abundances were detected in *Tollo* mutant embryos (see Fig. S7 in the supplementary material). The inability of transcriptional changes to account for the nature of the shift in glycan expression indicates that modulation of enzyme production is not the primary mechanism by which *sff* alters N-glycosylation.

Sff modulates Golgi compartmentation in neurons

Protein glycosylation reflects Golgi dynamics. Therefore, we hypothesized that Sff participates in the establishment of or trafficking through Golgi compartments. The *Drosophila* Golgi apparatus is striking for its lack of morphological similarity to classic conceptualizations of the ribbon-like stacked cisternae evident in many vertebrate cell types. Instead, the *Drosophila* Golgi exists as distributed puncta, forming multiple organelles within a single cell (Kondylis and Rabouille, 2009; Stanley et al., 1997). As the major change in *sff* N-glycan expression is a shift towards greater complexity, we focused first on late Golgi compartments using markers described previously to delineate the medial/trans and trans-Golgi in *Drosophila* (LaJeunesse et al., 2004; Yano et al., 2005). We assessed the relative distributions of Golgi-YFP (a medial/trans marker, YFP fused to the transmembrane localization domain of human β4GalT), *Arachis hypogaea* lectin (PNA) binding (a trans marker, Galβ3GalNAc specific lectin) and a neuronal protein (Fasciclin 2, Fas2) that bears an HRP epitope (Desai et al., 1994; Lin et al., 1994).

In triple-stained preparations (Golgi-YFP, PNA, Fas2), Golgi puncta were distributed throughout the nerve cord (see Fig. S9 in the supplementary material). Colocalized fluorescence intensity for each marker was quantified across all of the objects imaged within regions of interest in the ventral nerve cord (Fig. 7A-I and see Fig. S10 in the supplementary material). Colocalization of Fas2 with the trans marker demonstrates a striking change in the association of the HRP-bearing glycoprotein with this compartment of the Golgi (compare Fig. 7A with 7B, quantified in 7C). Essentially, all of the quantified Fas2 fluorescence intensity colocalized with the trans marker in *sff* mutants. The differential colocalization of Fas2 in *sff*

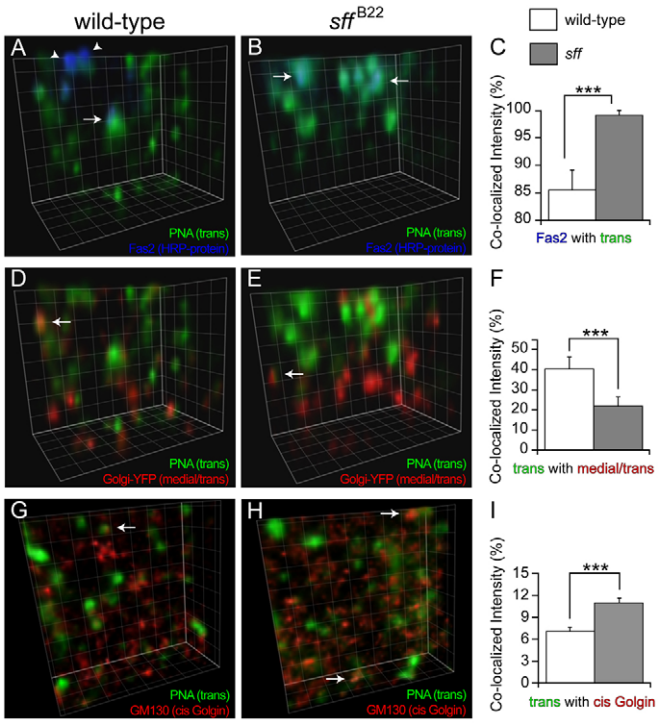

Fig. 7. Neuronal Golgi compartmentation is altered in *sff*^{B22}. (**A-F**) Representative three-dimensional reconstructions are shown of portions of regions of interest that were used to quantify Golgi marker colocalization in the ventral nerve cord of wild-type (A,D,G) and *sff*^{B22} (B,E,H) *Drosophila* embryos. Preparations were triple stained with PNA lectin (a trans Golgi marker; green), mAb 1D4 (Fas2, an HRP protein; blue) and anti-YFP (a medial/trans Golgi marker; red). Objects labeled for Fas2 and the trans marker are closely apposed (arrows in A) but exhibit less overlap in the wild-type nerve cord (arrowheads in A) than in the *sff*^{B22} mutant (B). Almost all the Fas2 signal overlaps with the trans marker in the mutant (arrows in B). Fluorescence intensity colocalization was quantified (C) within regions of interest for wild-type and *sff*^{B22} mutant embryos (mean ± s.e.m. for *n*=24 segments for each genotype). Fas2 signal is tightly associated with the trans marker in *sff*^{B22} [mean Pearson's correlation coefficient (PCC)=0.62±0.14], demonstrating a statistically significant increase over the colocalization of these markers in wild type (PCC=0.45±0.12). Consistent with increased polarization between Golgi compartments, trans and medial/trans markers display less overlap in *sff*^{B22} mutant embryos (arrows in D and E, quantified in F, PCC=0.19±0.03 and 0.31±0.05 in *sff*^{B22} and wild type, respectively, *n*=24 segments for each genotype). (**G-I**) Preparations were double stained (G,H) with PNA lectin (green) and anti-GM130 (a Golgin localized to the cis Golgi; red). Unlike the medial/trans marker, the cis marker GM130 displays increased overlap with the trans compartment in *sff*^{B22} mutant embryos (arrows in G and H, quantified in I; PCC=0.46±0.14 and 0.05±0.03 in *sff*^{B22} and wild type, respectively, *n*=12 segments for wild-type and *n*=7 segments for *sff*^{B22}). Regions of interest were selected to eliminate any contribution of axon staining to the final quantification (see Figs S9, S10 in the supplementary material). Gridlines correspond to 1 μm in all reconstructions. ***P<0.002.

mutants indicates that the cisternal association of this glycoprotein has shifted towards a later compartment, away from the earlier localization expected for enzymes that generate paucimannose-type glycans (including simple HRP epitopes) and towards the localization expected for later-processing enzymes involved in complex branching (GlcNAcT2, GlcNAcT4). Consistent with increased polarization between late Golgi compartments, the *sff* mutation caused greater segregation of trans and medial/trans markers (compare Fig. 7D with 7E, quantified in 7F).

To examine the integrity of the early Golgi in *sff* mutants, we assessed the distribution of GM130, a cis-localized Golgin (Nakamura et al., 1997). Overlap between the trans marker and GM130 was low in wild-type and *sff* mutant embryos. However, the mutant displayed a statistically significant increase in colocalization, indicating that this Golgi matrix component had expanded into the cisternal territory from which it is normally restricted (Fig. 7G-I).

DISCUSSION

Tissue-specific protein glycosylation requires coordinated trafficking of substrates and modifying enzymes through Golgi compartments

We have presented data demonstrating that a mutation in *Drosophila* Sff alters glycan expression in the embryonic nervous system. The neural-specific N-linked glycans known as HRP epitopes are reduced in sff mutant embryos and the expression of a subset of complex glycans is increased. Protein kinases have previously been linked to altered glycosylation, based primarily on pharmacological manipulations in cultured cells (Yu and Bieberich, 2001). For example, treatment of NRK cells with activators of protein kinase A alters vesicular stomatitis virus G protein glycosylation in infected cells (Muniz et al., 1996; Muniz et al., 1997). Furthermore, protein kinase C activity modulates sialylation of glycosphingolipids in NG108-15 and of glycoproteins in SH-SY5Y, as well as polysialylation of NCAM in neuro-2A and PC-12 cells (Bieberich et al., 1998; Breen and Georgopoulou, 2003; Gallagher et al., 2000). However, the functional consequences of these pharmacological effects have not been validated in vivo, nor have molecular or cellular mechanisms underlying altered glycosylation been identified.

The expression of *Drosophila* HRP epitopes is not only tissue-restricted, it is also protein-restricted in wild-type embryos; only a subset of neuronal proteins bears α3-fucosylated glycans (Desai et al., 1994). The influence of α3-fucosylation on the function of any of the individual proteins that carry this specific post-translational modification is currently unknown; the glycan might influence protein stability or protein interactions, or serve as a recognition marker independent of the protein on which it resides. Regardless of its function, the tissue-specificity of HRP-epitope expression in the *Drosophila* embryo provides a platform for assessing the regulatory mechanisms that control glycosylation in vivo. In general, the regulation of glycosylation, and particularly of glycan diversity on specific proteins, is multi-dimensional. The coordinated expression of appropriate glycosyltransferases and target proteins alone is insufficient for achieving specific glycosylation. Target and enzyme must also be brought together within a permissive Golgi domain, which must contain other supporting activities, such as appropriate nucleotide sugar transporters and trimming exoglycosidases.

The multidimensionality of regulated glycan expression means that Sff might influence protein glycosylation at any of several control points. The kinase might modulate the expression of glycan modifying enzymes, but our analysis of glycogene transcript levels in the *sff* mutant indicates that the expression of glycosyltransferases and glycan processing enzymes cannot account for the observed shifts in glycan prevalence. Differential lysosomal degradation of specific protein glycoforms could also generate a shift in glycan profiles, but altered catabolism cannot

explain the increase in complex glycans observed in the *sff* mutant. Finally, glycosyltransferase phosphorylation has been described in vitro, but evidence for a functional consequence of this modification is currently lacking (Gallagher et al., 2001; Hathaway et al., 2003; Ma et al., 1999). The hypothesis most consistent with our results is that Sff modulates glycan processing by influencing the compartmentation of glycan processing within the Golgi apparatus.

Very little is known regarding the coordinated Golgi dynamics that produce the confluence of components necessary for specific glycan expression in embryos or in mature tissues (Gerardy-Schahn et al., 2001; Nilsson et al., 2009), but a specific role for protein phosphorylation in controlling Golgi function is not without precedent. The cyclin-dependent kinase Cdk1-cyclin B initiates the process of Golgi disassembly during mitosis by phosphorylating Rab1 and Golgin GM130, which together recruit an ER-derived vesicle tethering factor (p115) to cis-Golgi membranes (Misteli and Warren, 1995). Other kinases, including polo-like kinases, extracellular signal-regulated kinases and mitogen-activated protein kinases, function along with Cdk1-cyclin B to dismantle the Golgi during mitosis, and additional kinases contribute to bulk Golgi trafficking during interphase or modulate vesicle coat assembly (Dirac-Svejstrup et al., 2000; Doray et al., 2002; Preisinger and Barr, 2005). In these examples of full Golgi collapse, Golgi partition during mitosis and vesicle coat disruption, kinase activities initiate dramatic Golgi remodeling events. The Sff function that we have described is more restricted, impacting a subset of relatively minor glycan structures primarily associated with the late Golgi. Thus, the relative dosage of specific kinases, within a larger ensemble of phosphorylating enzymes, might sculpt unique glycan expression profiles in specific cell types through targeted modulation of Golgi compartmentation.

Based on the function of SAD kinase at the mature synapse, where it facilitates tethering of vesicles to membrane-associated protein complexes, and on the narrowly distributed changes in the N-glycan profile of *sff* mutant embryos, we propose that Sff kinase activity modulates Golgi vesicle interactions within a subset of cisternal membranes (Fig. 8). Our glycan characterization indicates that appropriate targeting of these vesicles normally limits the expansion of N-linked glycan complexity and facilitates the generation of HRP epitopes in neural tissue. When *sff* activity is reduced, some glycoprotein substrates gain access to alternative Golgi processing enzymes and the loss in tethering specificity generates a shift in Golgi vesicle trafficking.

Molecular targets for Sff at the Golgi apparatus and signaling pathways that impinge upon tissue-specific glycosylation

Vesicular capture at presynaptic membranes requires the interaction of specific Rab GTPase proteins and scaffolding/tethering factors (Inoue et al., 2006; Schoch et al., 2002; Sinka et al., 2008). Vesicular transport through the Golgi apparatus is also modulated by interactions between Rab proteins and tethering factors (Ren et al., 2009; Sztul and Lupashin, 2009). The Golgins, which exhibit compartment-specific distributions across the Golgi, are a component of the mechanism that imparts specificity to vesicle-target recognition (Short et al., 2005). Structural analysis predicts that the Golgins are extended molecules that reach into the surrounding cytoplasm from the Golgi membranes to which they are attached, providing a matrix for interaction and tethering of transport vesicles. The glycosylation phenotype that we have quantified in our *Drosophila sff* mutant indicates that the stability or functional integrity of Golgin-Rab-vesicle complexes might be differentially influenced by the activity of specific kinases. Therefore, Golgins, Rabs and, possibly, components of the

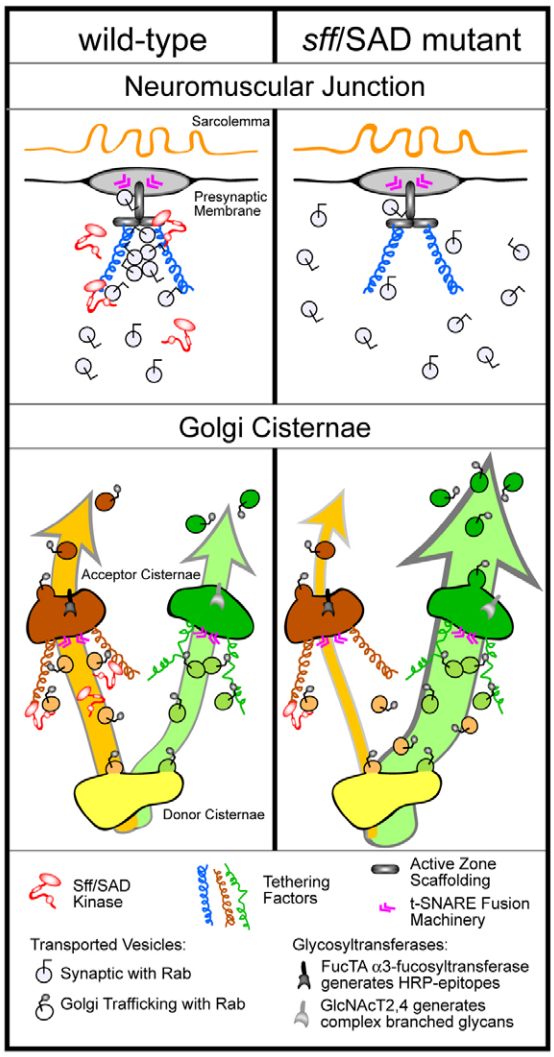

Fig. 8. Parallels between known functions for Sff/SAD at the presynaptic membrane of the neuromuscular junction (NMJ) and proposed functions for Sff/SAD at cisternal membranes of the Golgi apparatus. At the NMJ, SAD kinase facilitates the tethering of synaptic vesicles at presynaptic active zones. The tethering complex brings together molecular components necessary for priming and fusion of synaptic vesicles. Presynaptic tethering complexes comprise spatially extended tethering factors such as Bruchpilot (a *Drosophila* protein that combines the signature domains of the vertebrate Bassoon/Piccolo and ERKs/CAST family members) and other scaffold or tethering components. In the absence of SAD kinase, synaptic vesicles are inefficiently associated with the active zone. Altered glycan expression in the *Drosophila sff* mutant indicates that Sff/SAD kinase serves an analogous function at Golgi cisternal membranes, ensuring that specific Golgi transport vesicles associate with appropriate stack-specific tethering factors such as Golgin family members. In the *sff* mutant, Golgi vesicular transport is not halted because secondary cisternal targets are available and competent for fusion. But, the resulting aberrant trafficking shifts glycan profiles by allowing access of glycoprotein substrates to alternative ensembles of processing enzymes (Golgi glycosyltransferases). In sff^{B22}, decreased activity reduces HRP-epitope expression (orange processing pathway) and increases complex glycan production (green processing pathway).

retrograde transport machinery [conserved oligomeric Golgi (COG) and Golgi associated retrograde protein (GARP) complexes], are prime candidate substrates for phosphorylation by Sff. The modestly expanded distribution of a Golgin (GM130) in the nervous system of the *sff*^{B22} mutant is consistent with the hypothesis that Sff modulates tethering factor function and could suggest that GM130 is a substrate for the enzyme. However, altered GM130 distribution might also result from aberrant modulation of Rabs or downstream tethering factors. Further genetic, biochemical and proteomic analysis will be necessary to ascertain the identity of the Sff substrates most relevant for controlling the Golgi dynamics that regulate tissue-specific glycosylation.

SAD kinases belong to the AMP-activated protein kinase (AMPK)-sucrose non-fermenting 1 (SNF1) family of serine-threonine kinases, many of which convey signals that regulate cell polarity and energy utilization (Barnes et al., 2007; Carling et al., 1994; Kishi et al., 2005). Neuronal polarization defects are not apparent in our *sff* mutant embryo. The lack of gross polarity defects in *sff* might simply reflect the hypomorphic nature of our *sff*^{B22} allele, indicating that neuronal polarization requires less Sff protein than is necessary for establishing neuron-specific glycan expression. However, the sorting function of the Golgi apparatus is intimately associated with cell polarity. In some cases, the glycans on sorted proteins influence their sorting, linking the Golgi function that we have detected for Sff to cell polarity (Potter et al., 2006).

The reduction of *sff* mRNA in the *Tollo* mutant background implicates transcriptional control or message stability as a mechanism underlying neuron-specific glycan expression. Vertebrate SAD kinase expression is regulated through metabolic sensing pathways involving protein kinase B (AKT) inhibition of TSC1-TSC2 and activation of TORC1 (Wildonger et al., 2008). This paradigm nominates a range of survival/growth factors, hormones, neurotransmitters and other effectors of AKT or phosphoinositide 3-kinase (PI3K) activation as molecules capable of propagating the transcellular signal initiated by *Tollo* in *Drosophila*. In a broader context, our results provide a new mechanism for reinterpreting many years of empirical observations describing the impact of endocrine factors, tissue microenvironments and culture conditions on cellular protein glycosylation (Knezevic et al., 2009; Varki, 1993).

Acknowledgements

The authors gratefully acknowledge valuable consultations with L. Wells, R. Steet, P. Zhao, M. Ishihara, T. Katoh, A. Nairn and K. Moremen (CCRC, UGA). K. Habenicht, C. Hupman, M. Hirsu, R. Cantu, S. Lee and N. Price contributed essential technical support during implementation of the screen. We are extremely grateful to Bernard Charroux and Julien Royet (IBDM Luminy) for generously providing the *tollo*^{c5} mutant. This work was supported by NIH/NIGMS (GM072839 to M.T.), a Cousins Foundation Fellowship (to S.B.) and a Toyobo Biotechnology Foundation Long-term Research Grant (to K.A.). Deposited in PMC for release after 12 months.

Competing interests statement

The authors declare no competing financial interests.

Supplementary material

Supplementary material for this article is available at
http://dev.biologists.org/lookup/suppl/doi:10.1242/dev.055376/-/DC1

References

Acheson, A., Sunshine, J. L. and Rutishauser, U. (1991). NCAM Polysialic acid can regulate both cell-cell and cell-substrate interactions. *J. Cell Biol.* **114**, 143-153.

Allendoerfer, K. L., Durairaj, A., Matthews, G. A. and Patterson, P. H. (1999). Morphological domains of Lewis-X/FORSE-1 immunolabeling in the embryonic neural tube are due to developmental regulation of cell surface carbohydrate expression. *Dev. Biol.* **211**, 208-219.

Aoki, K., Perlman, M., Lim, J., Cantu, R., Wells, L. and Tiemeyer, M. (2007). Dynamic developmental elaboration of N-linked glycan complexity in the Drosophila melanogaster embryo. *J. Biol. Chem.* **282**, 9127-9142.

Barnes, A. P., Lilley, B. N., Pan, Y. A., Plummer, L. J., Powell, A. W., Raines, A. N., Sanes, J. R. and Polleux, F. (2007). LKB1 and SAD kinases define a pathway required for the polarization of cortical neurons. *Cell* **129**, 549-563.

Bieberich, E., Freischutz, B., Liour, S. S. and Yu, R. K. (1998). Regulation of ganglioside metabolism by phosphorylation and dephosphorylation. *J. Neurochem.* **71**, 972-979.

Brand, A. H., Manoukian, A. S. and Perrimon, N. (1994). Ectopic expression in *Drosophila*. In *Drosophila melanogaster: Practical Uses in Cell and Molecular Biology*, vol. 44 (ed. L. S. B. Goldstein and E. Fyrberg), pp. 635-654. San Diego: Academic Press.

Breen, K. C. and Georgopoulou, N. (2003). The role of protein phosphorylation in alpha2,6(N)-sialyltransferase activity. *Biochem. Biophys. Res. Commun.* **309**, 32-35.

Carling, D., Aguan, K., Woods, A., Verhoeven, A. J., Beri, R. K., Brennan, C. H., Sidebottom, C., Davison, M. D. and Scott, J. (1994). Mammalian AMP-activated protein kinase is homologous to yeast and plant protein kinases involved in the regulation of carbon metabolism. *J. Biol. Chem.* **269**, 11442-11448.

Constantine-Paton, M., Blum, A. S., Mendez-Otero, R. and Barnstable, C. J. (1986). A cell surface molecule distributed in a dorso-ventral gradient in the perinatal rat retina. *Nature* **324**, 459-462.

Crump, J., Zhen, M., Yishi, J. and Bargmann, C. (2001). The SAD-1 kinase regulates presynaptic vesicle clustering and axon termination. *Neuron* **29**, 115-129.

Dennis, J. W., Nabi, I. R. and Demetriou, M. (2009). Metabolism, cell surface organization, and disease. *Cell* **139**, 1229-1241.

Desai, C. J., Popova, E. and Zinn, K. (1994). A *Drosophila* receptor tyrosine phosphatase expressed in the embryonic CNS and larval optic lobes is a member of the set of proteins bearing the 'HRP' carbohydrate epitope. *J. Neurosci.* **14**, 7272-7283.

Dirac-Svejstrup, A. B., Shorter, J., Waters, M. G. and Warren, G. (2000). Phosphorylation of the vesicle-tethering protein p115 by a casein kinase II-like enzyme is required for Golgi reassembly from isolated mitotic fragments. *J. Cell Biol.* **150**, 475-488.

Doray, B., Ghosh, P., Griffith, J., Geuze, H. J. and Kornfeld, S. (2002). Cooperation of GGAs and AP-1 in packaging MPRs at the trans-Golgi network. *Science* **297**, 1700-1703.

Fabini, G., Freilinger, A., Altmann, F. and Wilson, I. B. (2001). Identification of core alpha 1,3 fucosylated glycans and cloning of the requisite fucosyltransferase cDNA from *Drosophila melanogaster*. Potential basis of the neural anti-horseradish peroxidase epitope. *J. Biol. Chem.* **276**, 28058-28067.

Freeze, H. H. (2002). Human disorders in N-glycosylation and animal models. *Biochim. Biophys. Acta* **1573**, 388-393.

Gallagher, H. C., Odumeru, O. A. and Regan, C. M. (2000). Regulation of neural cell adhesion molecule polysialylation state by cell-cell contact and protein kinase C delta. *J. Neurosci. Res.* **61**, 636-645.

Gallagher, H. C., Murphy, K. J., Foley, A. G. and Regan, C. M. (2001). Protein kinase C delta regulates neural cell adhesion molecule polysialylation state in the rat brain. *J. Neurochem.* **77**, 425-434.

Gerardy-Schahn, R., Oelmann, S. and Bakker, H. (2001). Nucleotide sugar transporters: biological and functional aspects. *Biochimie* **83**, 775-782.

Haines, N. and Irvine, K. D. (2005). Functional analysis of Drosophila beta1,4-N-acetylgalactosaminyltransferases. *Glycobiology* **15**, 335-346.

Hanks, S. K. and Hunter, T. (1995). The eukaryotic protein kinase superfamily: kinase (catalytic) domain structure and classification. *FASEB J.* **9**, 576-596.

Hathaway, H. J., Evans, S. C., Dubois, D. H., Foote, C. I., Elder, B. H. and Shur, B. D. (2003). Mutational analysis of the cytoplasmic domain of beta1,4-galactosyltransferase I: influence of phosphorylation on cell surface expression. *J. Cell Sci.* **116**, 4319-4330.

Heinemeyer, T., Wingender, E., Reuter, I., Hermjakob, H., Kel, A. E., Kel, O. V., Ignatieva, E. V., Ananko, E. A., Podkolodnaya, O. A., Kolpakov, F. A. et al. (1998). Databases on transcriptional regulation: TRANSFAC, TRRD and COMPEL. *Nucleic Acids Res.* **26**, 362-367.

Inoue, E., Mochida, S., Takagi, H., Higa, S., Deguchi-Tawarada, M., Takao-Rikitsu, E., Inoue, M., Yao, I., Takeuchi, K., Kitajima, I. et al. (2006). SAD: a presynaptic kinase associated with synaptic vesicles and the active zone cytomatrix that regulates neurotransmitter release. *Neuron* **50**, 261-275.

Jan, L. Y. and Jan, Y. N. (1982). Antibodies to horseradish peroxidase as specific neuronal markers in *Drosophila* and grasshopper embryos. *Proc. Natl. Acad. Sci. USA* **79**, 2700-2704.

Kaufmann, N., DeProto, J., Ranjan, R., Wan, H. and Van Vactor, D. (2002). Drosophila liprin-alpha and the receptor phosphatase Dlar control synapse morphogenesis. *Neuron* **28**, 27-38.

Kishi, M., Pan, Y. A., Crump, J. G. and Sanes, J. R. (2005). Mammalian SAD kinases are required for neuronal polarization. *Science* **307**, 929-932.

Knezevic, A., Polasek, O., Gornik, O., Rudan, I., Campbell, H., Hayward, C., Wright, A., Kolcic, I., O'Donoghue, N., Bones, J. et al. (2009). Variability,

heritability and environmental determinants of human plasma N-glycome. *J. Proteome Res.* **8**, 694-701.
Koles, K., Irvine, K. D. and Panin, V. M. (2004). Functional characterization of *Drosophila* sialyltransferase. *J. Biol. Chem.* **279**, 4346-4357.
Kondylis, V. and Rabouille, C. (2009). The Golgi apparatus: lessons from Drosophila. *FEBS Lett.* **583**, 3827-3838.
Kopczynski, C. C., Davis, G. W. and Goodman, C. S. (1996). A neural tetraspanin, encoded by late bloomer, that facilitates synapse formation. *Science* **271**, 1867-1870.
Kruse, J., Mailhammer, R., Wernecke, H., Faissner, A., Sommer, I., Goridis, C. and Schachner, M. (1984). Neural cell adhesion molecules and myelin-associated glycoprotein share a common carbohydrate moiety recognized by monoclonal antibodies L2 and HNK-1. *Nature* **311**, 153-155.
Kurosaka, A., Yano, A., Itoh, N., Kuroda, Y., Nakagawa, T. and Kawasaki, T. (1991). The structure of a neural specific carbohydrate epitope of horseradish peroxidase recognized by anti-horseradish peroxidase antiserum. *J. Biol. Chem.* **266**, 4168-4172.
LaJeunesse, D. R., Buckner, S. M., Lake, J., Na, C., Pirt, A. and Fromson, K. (2004). Three new Drosophila markers of intracellular membranes. *Biotechniques* **36**, 784-788, 790.
Lee, S. U., Grigorian, A., Pawling, J., Chen, I. J., Gao, G., Mozaffar, T., McKerlie, C. and Demetriou, M. (2007). N-glycan processing deficiency promotes spontaneous inflammatory demyelination and neurodegeneration. *J. Biol. Chem.* **282**, 33725-33734.
Leonard, R., Rendic, D., Rabouille, C., Wilson, I. B., Preat, T. and Altmann, F. (2006). The Drosophila fused lobes gene encodes an N-acetylglucosaminidase involved in N-glycan processing. *J. Biol. Chem.* **281**, 4867-4875.
Lim, J. M., Sherling, D., Teo, C. F., Hausman, D. B., Lin, D. and Wells, L. (2008). Defining the regulated secreted proteome of rodent adipocytes upon the induction of insulin resistance. *J. Proteome Res.* **7**, 1251-1263.
Lin, D. M., Fetter, R. D., Kopczynski, C., Grenningloh, G. and Goodman, C. S. (1994). Genetic analysis of Fasciclin II in Drosophila: defasciculation, refasciculation, and altered fasciculation. *Neuron* **13**, 1055-1069.
Ma, J., Simonovic, M., Qian, R. and Colley, K. J. (1999). Sialyltransferase isoforms are phosphorylated in the cis-medial Golgi on serine and threonine residues in their luminal sequences. *J. Biol. Chem.* **274**, 8046-8052.
Martin, V., Mrkusich, E., Steinel, M. C., Rice, J., Merritt, D. J. and Whitington, P. M. (2008). The L1-type cell adhesion molecule Neuroglian is necessary for maintenance of sensory axon advance in the Drosophila embryo. *Neural Dev.* **3**, 10.
Matani, P., Sharrow, M. and Tiemeyer, M. (2007). Ligand, modulatory, and co-receptor functions of neural glycans. *Front. Biosci.* **12**, 3852-3879.
Mathew, S. J., Kerridge, S. and Leptin, M. (2009). A small genomic region containing several loci required for gastrulation in Drosophila. *PLoS ONE* **4**, e7437.
Matthews, R. T., Kelly, G. M., Zerillo, C. A., Tiemeyer, M. and Hockfield, S. (2002). Aggrecan glycoforms contribute to the molecular heterogeneity of perineuronal nets. *J. Neurosci.* **22**, 7536-7547.
Merritt, D. J. and Whitington, P. M. (1995). Central projections of sensory neurons in the Drosophila embryo correlate with sensory modality, soma position, and proneural gene function. *J. Neurosci.* **15**, 1755-1767.
Michele, D. E. and Campbell, K. P. (2003). Dystrophin-glycoprotein complex: Post-translational processing and dystroglycan function. *J. Biol. Chem.* **278**, 15457-15460.
Misteli, T. and Warren, G. (1995). Mitotic disassembly of the Golgi apparatus in vivo. *J. Cell Sci.* **108**, 2715-2727.
Muniz, M., Alonso, M., Hidalgo, J. and Velasco, A. (1996). A regulatory role for cAMP-dependent protein kinase in protein traffic along the exocytic route. *J. Biol. Chem.* **271**, 30935-30941.
Muniz, M., Martin, M. E., Hidalgo, J. and Velasco, A. (1997). Protein kinase A activity is required for the budding of constitutive transport vesicles from the trans-Golgi network. *Proc. Natl. Acad. Sci. USA* **94**, 14461-14466.
Nairn, A. V., Kinoshita-Toyoda, A., Toyoda, H., Xie, J., Harris, K., Dalton, S., Kulik, M., Pierce, J. M., Toida, T., Moremen, K. W. et al. (2007). Glycomics of proteoglycan biosynthesis in murine embryonic stem cell differentiation. *J. Proteome Res.* **6**, 4374-4387.
Nakamura, N., Lowe, M., Levine, T. P., Rabouille, C. and Warren, G. (1997). The vesicle docking protein p115 binds GM130, a cis-Golgi matrix protein, in a mitotically regulated manner. *Cell* **89**, 445-455.
Nilsson, T., Au, C. E. and Bergeron, J. J. (2009). Sorting out glycosylation enzymes in the Golgi apparatus. *FEBS Lett.* **583**, 3764-3769.
Okajima, T. and Irvine, K. D. (2002). Regulation of notch signaling by o-linked fucose. *Cell* **111**, 893-904.
Parks, A. L., Cook, K. R., Belvin, M., Dompe, N. A., Fawcett, R., Huppert, K., Tan, L. R., Winter, C. G., Bogart, K. P., Deal, J. E. et al. (2004). Systematic generation of high-resolution deletion coverage of the Drosophila melanogaster genome. *Nat. Genet.* **36**, 288-292.
Patel, N. H. (1994). Imaging Neuronal Subsets and Other Cell Types in Whole Mount *Drosophila* Embryos and Larvae Using Antibody Probes. In *Drosophila melanogaster: Practical Uses in Cell and Molecular Biology*, vol. 44 (ed. L. S. B. Goldstein and E. Fyrberg), pp. 445-487. San Diego: Academic Press.
Potter, B. A., Hughey, R. P. and Weisz, O. A. (2006). Role of N- and O-glycans in polarized biosynthetic sorting. *Am. J. Physiol. Cell Physiol.* **290**, C1-C10.
Preisinger, C. and Barr, F. A. (2005). Kinases regulating Golgi apparatus structure and function. *Biochem. Soc. Symp.* **72**, 15-30.
Ren, Y., Yip, C. K., Tripathi, A., Huie, D., Jeffrey, P. D., Walz, T. and Hughson, F. M. (2009). A structure-based mechanism for vesicle capture by the multisubunit tethering complex Dsl1. *Cell* **139**, 1119-1129.
Rendic, D., Linder, A., Paschinger, K., Borth, N., Wilson, I. B. and Fabini, G. (2006). Modulation of neural carbohydrate epitope expression in Drosophila melanogaster cells. *J. Biol. Chem.* **281**, 3343-3353.
Rendic, D., Sharrow, M., Katoh, T., Overcarsh, B., Nguyen, K., Kapurch, J., Aoki, K., Wilson, I. B. and Tiemeyer, M. (2010). Neural-specific alpha3-fucosylation of N-linked glycans in the Drosophila embryo requires fucosyltransferase A and influences developmental signaling associated with O-glycosylation. *Glycobiology* **20**, 1353-1365.
Repnikova, E., Koles, K., Nakamura, M., Pitts, J., Li, H., Ambavane, A., Zoran, M. J. and Panin, V. M. (2010). Sialyltransferase regulates nervous system function in Drosophila. *J. Neurosci.* **30**, 6466-6476.
Sanes, J. R., Schachner, M. and Covault, J. (1986). Expression of several adhesive macromolecules (N-CAM, L1, J1, NILE, uvomorulin, laminin, fibronectin, and a heparan sulfate proteoglycan) in embryonic, adult, and denervated adult skeletal muscle. *J. Cell Biol.* **102**, 420-431.
Sarkar, M., Leventis, P. A., Silvescu, C. I., Reinhold, V. N., Schachter, H. and Boulianne, G. L. (2006). Null mutations in Drosophila N-acetylglucosaminyltransferase I produce defects in locomotion and a reduced life span. *J. Biol. Chem.* **281**, 12776-12785.
Schnitzer, J. and Schachner, M. (1982). Cell type specificity of a neural cell surface antigen recognized by the monoclonal antibody A2B5. *Cell Tissue Res.* **224**, 625-636.
Schoch, S., Castillo, P. E., Jo, T., Mukherjee, K., Geppert, M., Wang, Y., Schmitz, F., Malenka, R. C. and Sudhof, T. C. (2002). RIM1alpha forms a protein scaffold for regulating neurotransmitter release at the active zone. *Nature* **415**, 321-326.
Seppo, A., Matani, P., Sharrow, M. and Tiemeyer, M. (2003). Induction of neuron-specific glycosylation by Tollo/Toll-8, a *Drosophila* Toll-like receptor expressed in non-neural cells. *Development* **130**, 1439-1448.
Short, B., Haas, A. and Barr, F. A. (2005). Golgins and GTPases, giving identity and structure to the Golgi apparatus. *Biochim. Biophys. Acta* **1744**, 383-395.
Sinka, R., Gillingham, A. K., Kondylis, V. and Munro, S. (2008). Golgi coiled-coil proteins contain multiple binding sites for Rab family G proteins. *J. Cell Biol.* **183**, 607-615.
Snow, P. M., Patel, N. H., Harrelson, A. L. and Goodman, C. S. (1987). Neural-specific carbohydrate moiety shared by many surface glycoproteins in *Drosophila* and grasshopper embryos. *J. Neurosci.* **7**, 4137-4144.
Stanley, H., Botas, J. and Malhotra, V. (1997). The mechanism of Golgi segregation during mitosis is cell type-specific. *Proc. Natl. Acad. Sci. USA* **94**, 14467-14470.
Sztul, E. and Lupashin, V. (2009). Role of vesicle tethering factors in the ER-Golgi membrane traffic. *FEBS Lett.* **583**, 3770-3783.
Varki, A. (1993). Biological roles of oligosaccharides. *Glycobiology* **3**, 97-130.
Vyas, A. A., Patel, H. V., Fromholt, S. E., Heffer-Lauc, S. E., Vyas, K. A., Dang, J., Schachner, M. and Schnaar, R. L. (2002). Gangliosides are functional nerve cell ligands for myelin-associated glycoprotein (MAG). *Proc. Natl. Acad. Sci. USA* **99**, 8412-8417.
Wagh, D. A., Rasse, T. M., Asan, E., Hofbauer, A., Schwenkert, I., Dürrbeck, H., Buchner, S., Dabauvalle, M. C., Schmidt, M., Qin, G. et al. (2006). Bruchpilot, a protein with homology to ELKS/CAST, is required for structural integrity and function of synaptic active zones in Drosophila. *Neuron* **49**, 833-844.
Wildonger, J., Jan, L. Y. and Jan, Y. N. (2008). The Tsc1-Tsc2 complex influences neuronal polarity by modulating TORC1 activity and SAD levels. *Genes Dev.* **22**, 2447-2453.
Yano, H., Yamamoto-Hino, M., Abe, M., Kuwahara, R., Haraguchi, S., Kusaka, I., Awano, W., Kinoshita-Toyoda, A., Toyoda, H. and Goto, S. (2005). Distinct functional units of the Golgi complex in Drosophila cells. *Proc. Natl. Acad. Sci. USA* **102**, 13467-13472.
Yu, R. K. and Bieberich, E. (2001). Regulation of glycosyltransferases in ganglioside biosynthesis by phosphorylation and dephosphorylation. *Mol. Cell. Endocrinol.* **177**, 19-24.
Zak, B. M., Crawford, B. E. and Esko, J. D. (2002). Hereditary multiple exostoses and heparan sulfate polymerization. *Biochim. Biophys. Acta* **1573**, 346-355.

Table S1. Viability of *sff* homozygotes

Genotype	Number of embryos at start	Number of pupae	% of expected	Number of adults	% of expected
wild type	457	373	82	364	80
sff ^{B22}	560	219	39	207	37

'% of expected' for each genotype at each stage is calculated relative to the 'Number of embryos at start'

Table S2. PCR primer sequences

PCR primer sequences for mapping deletion breakpoints

Gene	Sense	Antisense
CG9122 (Trh)	CTAGCCATTGAATACATCACCAGATCGG	GCCAAGTGAATTGTACTACGCATACACCT
CG5942 (Brm)	CTTGCGGTAACCCTCCTCATCC	GCCAGCATGCAGGACAACC
CG32155	CGCGACTGAACAGTTATGATCG	CGGTGATGGATGCAAACAGG
CG13055	CCTTTGAGATATGTGTAGGAGACG	GGAAATTAAGCACACGCACG
CG13073	GCTGCGATTTGTGCTTATTCC	GCCTCGCAGATATAGATATAGATGG
CG6117 (Pka-C3)	CCACTCCAAATATCAAGATTTACCG	GCCAGCAGAAGCATCATTATTACC
CG33989 (pHCl)	GGAAGTTGGGTGGGCTTATGC	GGCATACGGGCAATGTGACC
CG6114 (Sff/SAD)	GCATTCAAAGTGCCTGGTGC	GGTGGAGCACAGGAGTACATGG
CG6114 (Sff/SAD)	GCGATTGGAGTTTAGTTTGCAGAGC	GCACAGCACATGCCCTAATAAAGC

PCR primer sequences for qRT-PCR

Gene	Sense	Antisense
GAPDH1	CTCCGTTGTGGATCTTACCG	CGACCTTAGCCTTGATTTCG
Fused lobes	TGCGGTGACGTTAACATTTG	CTGTGCGTCTGAGAGCTGAG
FucTA	GAAAGTGGCCTGGTTTGTGT	AGCTCATGGGCATACTGGAG
GlcNAcT1	GCGTAGGCAGGAGTACTTGG	CTAGGGATCTGGAGCAGACG
GlcNAcT2	CTGGTGTTCTCGCACGACTA	CATCACCTTGCAGAAGTCGA
CG9384 (GlcNAcT4)	GCAATCGTACCTCCTTGGAA	GTTTCGTTCTGCTCCTCGTC
CG6114 (Sff/SAD)	AACCAACTAGCGAACGAATCA	TGAAGATCTCTGGCTGATGGT

PCR primer sequences for in situ hybridization probes

Gene	Sense	Antisense
CG6114 (Sff/SAD)	CGCTGCTCATTGCACAGTGC	GCTGAGCACGAACGCAACC

Primer sequences are given in 5′-3′ direction.

Table S3. Proteomic analysis of wild-type and *sff* adult heads

Protein	Peptides	Genotype	Charge	XCorr
Endoribonuclease Dcr-1 (Control)	LEFLGDAVLDYLITRHLYEDPR*	wild-type	2	2.0
		sff ^{B22}	2	1.5
Guanine nucleotide releasing factor 2 (Control)	NISHSQTMNIMPMSK*	wild-type	2	1.0
		sff ^{B22}	2	1.6
Sff peptides with Xcorr ≥ 1.2 in wild type or *sff*	RQVIENDMENDSIFSYK*	wild-type	2	2.2
		sff ^{B22}	nd	
	IERRDSLR	wild-type	2	1.6
		sff ^{B22}	nd	
	LGVHVIGK[†]	wild-type	2	1.2
		sff ^{B22}	2	0.5
	VEREIAIMK[‡]	wild-type	2	0.8
		sff ^{B22}	2	1.6
	LEKTLGKGQTGLVK	wild-type	2	0.7
		sff ^{B22}	2	1.3
Sff peptides with Xcorr<1.2	17 additional peptides	wild-type	1-5	<1.2
	6 additional peptides[§]	*sff* ^{B22}	1-2	<1.2

nd denotes that the peptide was not detected in *sff* mutant.

*See Fig. S6 in the supplementary material for LC-MS/MS base peak chromatograms.

[†]Detected as its carbamidomethylated form in wild type and as a missed cleavage (LGVHVIGKKVAIK) in *sff* mutant.

[‡]Oxidized in wild type.

[§]Two of the six additional peptides detected in *sff* mutant heads were also detected in wild type.

Table S4. N-linked glycan profiles of wild-type and *sff* embryos

	Structure		% of total profile	
			wild type	*sff*^{B22}
1	M2N2		2.7±0.6	3.8±0.4
2	M3N2		7.3±1.0	9.6±1.4
3	M4N2	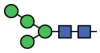	3.0±0.3	3.0±0.6
4	M5N2	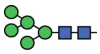	13.4±0.1	9.8±1.6
5	M6N2		10.4±0.3	10.4±1.5
6	M7N2	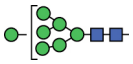	8.0±0.8	8.8±1.2
7	M8N2	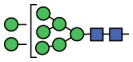	7.6±0.6	7.7±1.4
8	M9N2	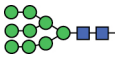	12.6±1.1	11.4±3.4
9	GlcM9N2	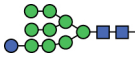	2.4±0.2	2.2±0.7
10	M2N2F$^{3 \text{ or } 6}$		8.0±0.4	9.1±1.2
11	M3N2F$^{3 \text{ or } 6}$		12.8±0.7	11.7±1.7
12	M4N2F^{6}	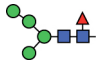	1.0±0.1	0.64±0.05
13	M5N2F^{6}	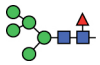	0.26±0.07	0.26±0.09
14	NM2N2F^{6}	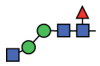	0.16±0.03	0.15±0.03
15	NM3N2F^{6}	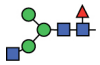	1.7±0.2	1.8±0.5
16	NM4N2F^{6}	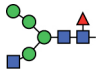	0.26±0.07	0.5±0.1
17	NM5N2F^{6}	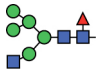	0.26±0.06	0.54±0.08
18	GalNM3N2F^{6}	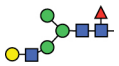	0.08±0.01	0.07±0.06
19	Hex-GalNM3N2F^{6}	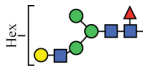	0.02±0.00	0.02±0.01
20	N2M2N2F^{6}	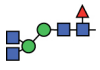	0.20±0.02	0.31±0.09
21	N2M3N2F^{6}	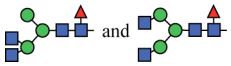	0.89±0.11	0.74±0.08

	Structure		% of total profile	
			wild type	*sff*^{B22}
22	N2M4N2F^{6}	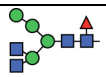	0.24±0.06	0.37±0.10
23	N2M5N2F^{6}	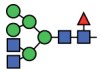	0.06±0.02	0.28±0.04
24	N3M3N2F^{6}	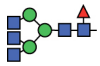	0.14±0.04	0.54±0.12
25	GalN2M3N2F^{6}	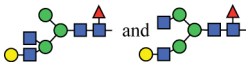	0.04±0.02	0.03±0.01
26	M2N2F2^{3,6}		0.24±0.02	0.02±0.01
27	M3N2F2^{3,6}		0.34±0.05	0.20±0.09
28	NM3N2F2^{3,6}	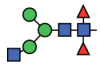	0.13±0.03	0.01±0.00
29	GalNM3N2F2^{3,6}	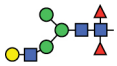	0.01±0.00	<0.01
30	N2M3N2F2^{3,6}	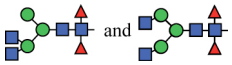	0.06±0.01	0.10±0.2
31	NM2N2	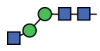	0.08±0.02	0.02±0.01
32	NM3N2	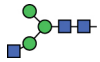	1.8±0.2	1.7±0.3
33	NM4N2	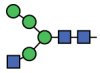	0.74±0.06	1.0±0.1
34	NM5N2	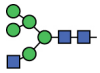	0.99±0.12	1.0±0.2
35	GalNM3N2	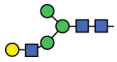	0.31±0.02	0.07±0.02
36	N2M3N2	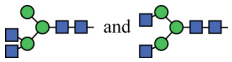	0.77±0.12	1.0±0.2
37	N2M4N2	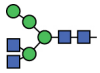	0.41±0.02	0.48±0.20
38	N2M5N2	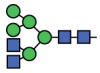	0.22±0.04	0.32±0.08
39	N3M3N2	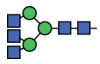	0.08±0.01	0.05±0.04
40	GalN2M3N2	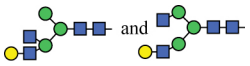	0.10±0.04	0.01±0.01
41	SA-GalNM3N2		0.02±0.01	0.01±0.01
42	SA-GalN2M3N2		0.01±0.00	0.03±0.01

The prevalence of each glycan structure is given as '% total profile', where the signal or each individual glycan is normalized to the total signal for all quantified glycans. Values are the mean ± s.e.m. for three independent determinations (biological replicates). For structures linked by 'and' both isomers were detected. For structures linked by 'or' the isomers were not resolved. Graphical glycan representations are consistent with the conventions proposed by the Consortium for Functional Glycomics, as follows: